ARTICLES

Measurement of Clathrate Hydrates via Raman Spectroscopy

Amadeu K. Sum, Robert C. Burruss,† and E. Dendy Sloan, Jr.*

Center for Hydrate Research, Department of Chemical Engineering, Colorado School of Mines, Golden, Colorado 80401

Received: February 28, 1997; In Final Form: June 11, 1997[⊗]

Raman spectra of clathrate hydrate guest molecules are presented for three known structures (**I** (**sI**), **II** (**sII**), and **H** (**sH**)) in the following systems: CH_4 (**sI**), CO_2 (**sI**), C_3H_8 (**sII**), $CH_4 + CO_2$ (**sI**), $CD_4 + C_3H_8$ (**sII**), $CH_4 + N_2$ (**sI**), CH_4 + THF-d_8 (**sII**), and $CH_4 + C_7D_{14}$ (**sH**). Relative occupancy of CH_4 in the large and small cavities of **sI** were determined by deconvoluting the ν_1 symmetric bands, resulting in hydration numbers of 6.04 ± 0.03. The frequency of the ν_1 bands for CH_4 in structures I, II, and H differ statistically, so that Raman spectroscopy is a potential tool to identify hydrate crystal structure. Hydrate guest compositions were also measured for two vapor compositions of the $CH_4 + CO_2$ system, and they compared favorably with predictions. The large cavities were measured to be almost fully occupied by CH_4 and CO_2, whereas only a small fraction of the small cavities are occupied by CH_4. No CO_2 was found in the small cavities. Hydration numbers from 7.27 to 7.45 were calculated for the mixed hydrate.

Introduction

Methane is the most abundant hydrocarbon in natural gas and is commonly the dominant component of clathrate hydrates (gas hydrates) formed by hydrocarbon-rich natural gases either in nature or in industrial processes. Because of its relatively small molecular diameter, methane can occur in all three known gas hydrate structures.

In an attempt to more fully understand the thermodynamics and kinetics of gas hydrate formation and decomposition, we began investigating the use of Raman spectroscopy to analyze the composition of the solid hydrate phase at in-situ temperature and pressures. Our initial two-year effort by X. Long[1] was to measure Raman spectra of tetrahydrofuran (THF) clathrates and THF + water mixtures. This report summarizes our results with the follow-on study of methane bearing hydrates of structures I, II, and H.

Experimental Methods

Apparatus. The Raman spectrometer is an Instruments SA RAMANOR U-1000, 1m double-dispersed monochromator system equipped with 1800 grooves/mm holographic grating system. The spectra were recorded with a photomultiplier tube detector system. The excitation source was an Ar-ion laser emitting a 514.532 nm line and providing about 150 mW at the sample. The schematic of the system is shown in Figure 1. The Raman system was located at the U.S. Geological Survey, Denver, Colorado.

An IBM-XT computer with PRISM software provided control and data acquisition for the system. Routine calibration of the monochromator was done by using the 546.098 nm line of Hg, at 1123.4 cm^{-1} relative to the 514.532 nm green line of the Ar-ion laser. The scattered radiation was collected at the 90° geometry with slits set at 500 μm. Spectra were collected with a 0.5 cm^{-1} scanning step and 2.0 s integration time/step. Typically five scans were averaged to obtain each spectra.

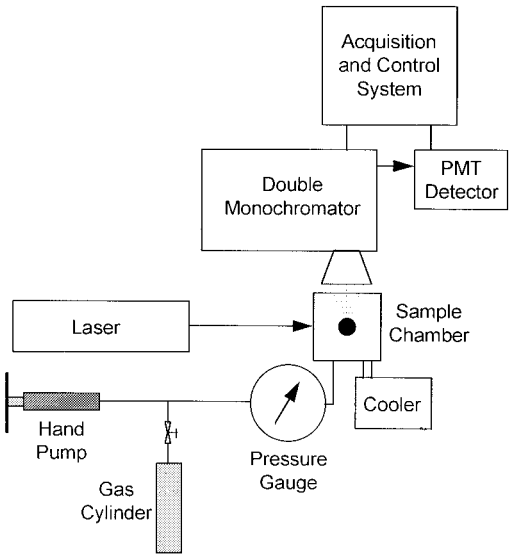

Figure 1. Schematic diagram of Raman spectrometer and sample control system

Hydrate samples and gas mixtures were prepared in a custom-designed high-pressure cell consisting of heavy-walled Pyrex capillary tube (2.0 mm i.d. × 6.4 mm o.d.) attached to a standard Swagelok "T" fitting. This design allowed us to operate at pressures to 14 MPa. One end of the Swagelok fitting was connected to the supply line while the other end was sealed. The glass capillary was surrounded by a glass jacket through which a water−methanol mixtures was circulated for temperature control. A small piece of magnetic wire was placed in the capillary to allow agitation of the water and gas mixture.

Procedure. Research grade (99.97%) methane (CH_4), instrumental grade (99.99%) carbon dioxide (CO_2), instrumental grade (99.5%) propane (C_3H_8), and research grade (99.8%) nitrogen (N_2) were acquired from General Air. Deuterated

† Energy Resources Program, United States Geological Survey, Box 25046-MS5973, Denver, Colorado 80225.

[⊗] Abstract published in *Advance ACS Abstracts,* August 1, 1997.

S1089-5647(97)00768-2 CCC: $14.00

methane (CD_4) was obtained from Isotec, Inc., containing 99.8% atom of isotopic enrichment and 99.4% chemical purity. Deuterated tetrahydrofuran (THF-d_8) of 99% atom deuterium and deuterated methylcyclohexane (C_7D_{14}) of 99% atom deuterium were acquired from Aldrich Chemical CO., Inc. Double-distilled water was used to prepare hydrate crystals.

Gas mixtures of $CH_4 + CO_2$, $CH_4 + N_2$, and $CD_4 + C_3H_8$ were prepared gravimetrically in a 300 mL stainless steel cylinder. The mixtures were thermally mixed with an infrared light source before use in the preparation of hydrate samples. Gas mixture composition uncertainty was 1 mol %.

Hydrate samples were prepared by injecting about 0.05 mL of water in the cell which was sealed and charged with a gas or gas mixture just above the equilibrium pressure. The cell was then immersed in a temperature-controlled bath, and hydrate nucleation and growth was promoted by periodic movement of the magnetic wire.

Samples for the $CH_4 + THF\text{-}d_8$ hydrate system were made by first mixing a solution of water and THF-d_8 close to the stoichiometric ratio (about 18:1). For the $CH_4 + C_7D_{14}$ hydrate system, water and an excess of C_7D_{14} were introduced separately into the cell since these two compounds are immiscible. Deuterated THF-d_8 and C_7D_{14} were used to prevent overlap between their normal CH stretching bands and the ν_1 band of CH_4. Similarly, the $CD_4 + C_3H_8$ system was studied to eliminate overlap between the CH stretching bands of the two components.

After hydrate formation, the cell was transported in an ice bath to the Raman spectroscopy laboratory located at the U.S. Geological Survey. Once the hydrate sample was set into the sample chamber of the spectrometer, the desired temperature and pressure (controlled by hand pump) were adjusted. The hydrate sample was then allowed to equilibrate for a period between several hours and a few days before measurement. The pressure was set to within 5% of the predicted equilibrium pressure at a given temperature, as calculated by CSMHYD.[2]

After spectra were collected at a single set of pressure−temperature conditions, the temperature and pressure were adjusted to a new equilibrium condition and hydrates reformed, with conditioning as before. All the hydrate measurements were performed at or above the ice point. When working with a gas mixture, the vapor composition was assumed to remain constant due to the large reservoir attached to the sample cell.

Once the cell was set in the sample chamber of the Raman spectrometer and hydrates conditioned, the position of the cell was translated in the $x-y-z$ directions to focus the laser beam at a specific hydrate mass in the sample to optimize the scattering response.

Theory and Calibration. This section provides background for later discussion on hydrate composition determination. A comprehensive description of the Raman scattering phenomena is given by D. Long.[3] The application of Raman spectroscopy to quantitative work has been limited by uncertainty in the determination of parameters underlying the polarizability theory and by practical limitations. A comprehensive analysis of the limitations of Raman spectroscopy to quantitative analysis was presented by Wopenka and Pasteris.[4] However, Wopenka and Pasteris also suggested a technique that enables the quantification of Raman bands via "Raman quantification factors".[5]

The polarizability theory described by Placzek[6] for the area A of a Raman band (defined over a finite range, $\bar{\nu}_1-\bar{\nu}_2$) is given by

$$A \propto \int_{\bar{\nu}_1}^{\bar{\nu}_2} \sigma_i(\bar{\nu}_o - \bar{\nu}_{vib})\mathrm{d}\bar{\nu} N(V) I(\bar{\nu}_o)\Omega \qquad (1)$$

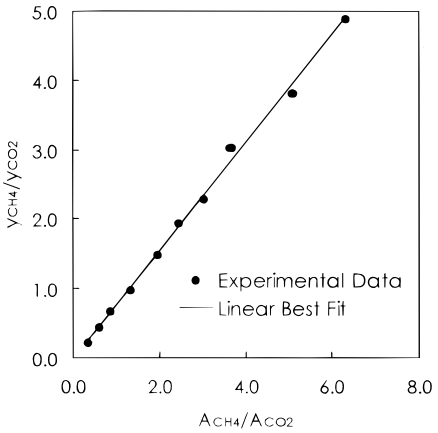

Figure 2. Calibration curve for $CH_4 + CO_2$ system based on vapor mixtures. Ordinate is mole fraction ratio of gas species. Abscissa is ratio of Raman peak areas.

where $\bar{\nu}_o$ = wavenumber of excitation line, $\bar{\nu}_{vib}$ = wavenumber of vibrational mode, σ_i = absolute Raman scattering cross section, $N(V)$ = density of molecules in scattering volume V, $I(\nu_o)$ = irradiance of species I, and Ω = angle of scattering geometry.

Consider a two-component system and apply the ratio method employed by Wopenka and Pasteris,[5] to obtain an expression relating the concentration C_i of species A and B to the measured Raman band areas (A_i), Raman cross sections (σ_i), and instrumental factors (η_i) by

$$\frac{C_A}{C_B} = \frac{A_A}{A_B}\frac{\sigma_B}{\sigma_A}\frac{\eta_B}{\eta_A} = \frac{A_A}{A_B} \times \frac{F_B}{F_A} \qquad (2)$$

The above equation is very similar to the familiar Beer's law for absorption:

$$\Xi = \epsilon b c \qquad (3)$$

Beer's law is extensively used in quantitative work to determine the concentration of a particular species by measuring the absorbance Ξ, knowing the molar absorptivity ϵ, and the pathlength b. However, the accurate measurement of both σ_i and η_i in eq 2 is very difficult, due to practical limitations such as the detector counting statistics and instrumental reproducibility. Most of the data available in the literature are for relative differential cross sections (to N_2), and even these show considerable variation, as reported by Schrötter and Klöckner.[7]

Therefore, by introducing the "Raman quantification factors" (F_i's), we combined σ_i and η_i to apply the same technique as in absorption studies, that is, to generate a calibration curve which is instrument dependent for the mixture of interest. Figure 2 is the calibration curve constructed for the $CH_4 + CO_2$ mixture, which relates area ratios to concentration ratios.

One important assumption built into the application of the calibration curve is that the Raman scattering cross sections of species do not change when incorporated into the hydrate lattice. The following reasoning was the basis for applying the calibration curve in Figure 2 (based on vapor species) to clathrated species. It is clear that molecules incorporated in the hydrate lattice (confined to the space inside a particular cavity) are in a different chemical environment from that of free molecules in the vapor phase. However, since small guest rotation and vibrations are not significantly restricted inside the lattice cavities, the major interaction between the gas molecules or between the gas and water molecules is via van der Waals forces. Therefore, we do not expect significant changes in the Raman scattering cross section of the gas molecules when

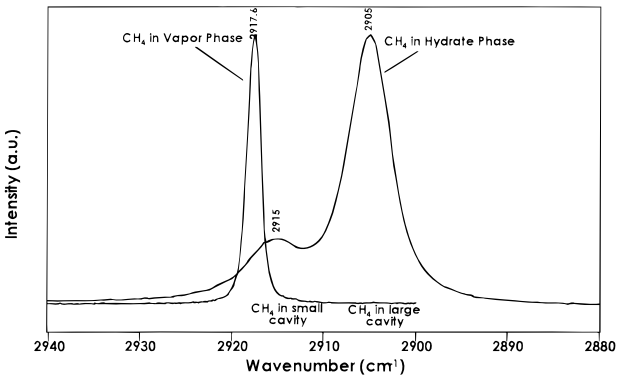

Figure 3. Raman spectra of the ν_1 stretching mode of CH_4 vapor at 33.6 bar and CH_4 incorporated into hydrate. Note that the CH_4 band for the hydrate is split into two peaks, indicating incorporation of CH_4 into both cavities of **sI** hydrate.

enclathrated in the hydrate (we are presently evaluating the magnitude of possible changes in the scattering cross section.)

Results and Discussion

Single Hydrates. Raman spectra for CH_4, CO_2, and C_3H_8 single hydrates were measured to determine the change in the vibrational frequency of the molecules when incorporated into the hydrate lattice. Only CH_4 hydrates were measured at equilibrium conditions, with liquid water, hydrate, and vapor phases coexisting. Carbon dioxide and propane hydrates were formed and measured at two-phase conditions so that the water phase was entirely depleted.

Figures 3−5 show the Raman spectra for CH_4, CO_2 and C_3H_8 hydrates, respectively. All three figures plot the spectra for the vapor and clathrated species. Figure 3 shows the ν_1 symmetric band of CH_4. The vibrational band for CH_4 in the clathrate is distinct from that for free vapor CH_4 (measured at room temperature and 33.6 bars). The splitting of the bands indicates that CH_4 partitions between the small (5^{12}) and large ($5^{12}6^2$) cavities of **sI**. By considering the intensity of the bands, we assigned the smaller band at high frequency to CH_4 in the small cavity and the larger band at lower frequency to CH_4 in the large cavity of **sI**. This reasoning is consistent with the density of cavities per unit cell of **sI**, which contains two small and six large cavities. The ratio of the small to the large bands in Figure 3 is very close to 1:3, which is the ratio of small to large cavities in the unit cell. We note that Seitz et al.[8] also observed splitting of the CH_4 band in the hydrate in their fluid inclusion work, however, their band assignment was counter to that suggested in this paper. Later in this section we provide further rationale for our assignment. Figure 3 shows only one of several samples of CH_4 hydrate, which was measured at $T = 273.6$ K. Spectra for other samples have identical features.

As seen in Figure 4, the Raman spectrum of CO_2 vapor (measured at room temperature and 33.6 bar) is composed of two major bands called the Fermi diad and two minor bands denoted as hot bands which are coupled through Fermi resonance. When CO_2 is incorporated into the hydrate lattice, the major bands are still very pronounced; however, the hot bands convolute into the Fermi diad bands, hence contributing to a tail of the bands. The CO_2 hydrate spectrum in Figure 4 is for a sample at a pressure above the three-phase equilibrium conditions. CO_2 forms type **sI** hydrate. Ratcliffe and Ripmeester[9] suggested that CO_2 only occupies the large cavity of **sI**. FTIR work by Fleyfel and Devlin[10] indicated the presence of CO_2 in the small cavity of **sI** in a mixed hydrate of CO_2 and ethylene oxide at very low temperature. However, our work

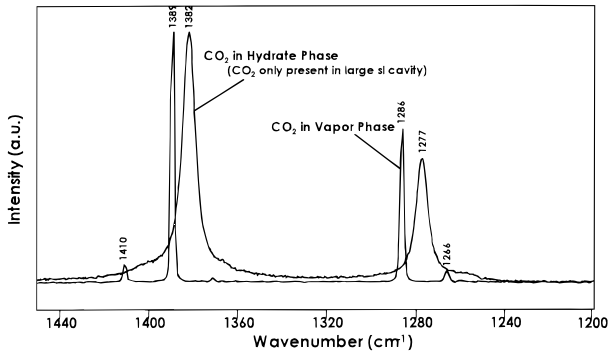

Figure 4. Raman spectra for the Fermi diad of CO_2 vapor and CO_2 incorporated into hydrate. Note broadening of the CO_2 bands in the hydrate phase. Lack of splitting of the bands suggests that CO_2 is present only in the large cavity of **sI** hydrate.

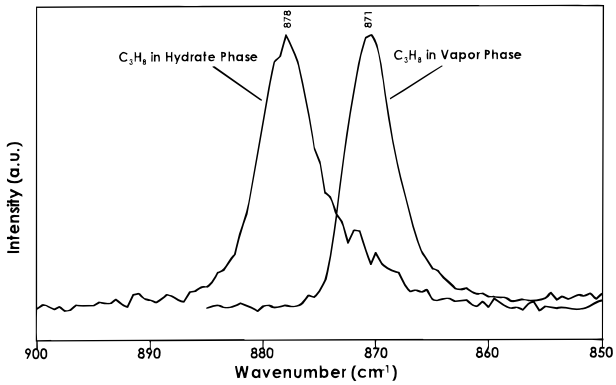

Figure 5. Raman spectra of the C−C stretch for C_3H_8 vapor and C_3H_8 incorporated into hydrate. Propane only occupies the large cavity of **sII** hydrate and therefore this band is not split.

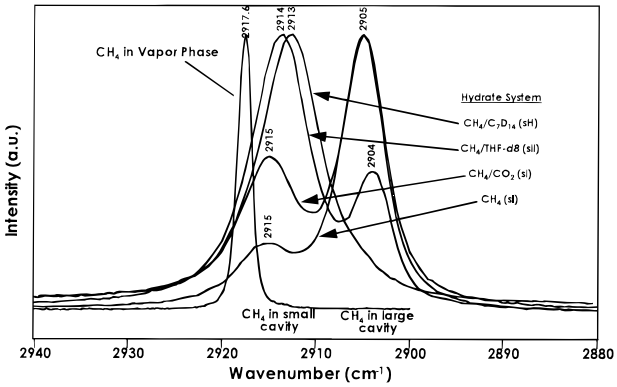

Figure 6. Raman spectra for CH_4 in double hydrates of **sI**, **sII**, and **sH**. A critical factor of this figure is the shift in peak position of CH_4 in the small cavities of **sI**, **sII**, and **sH** and in the large cavities of **sI** and **sII**. See text for further discussion.

does not indicate that CO_2 occupies the small cavity of **sI**, since we do not observe splitting of the CO_2 bands.

Propane forms **sII** hydrate crystals and can only occupy the large cavity ($5^{12}6^4$). Figure 5 shows the C−C stretch mode region for C_3H_8. The hydrate spectra was measured at pressures above the three-phase condition. The C_3H_8 hydrate spectrum in Figure 5 is shifted to higher wavenumbers relative to vapor C_3H_8 (measured at 273.6 K and 6.11 bars), whereas Figures 4 and 5 show that the bands for CH_4 and CO_2 in the hydrate are shifted to lower wavenumbers (different vibrational modes for CH_4, CO_2, and C_3H_8, are affected differently in the confined space inside the clathrate cavities).

Double Hydrates. All the double-hydrate systems chosen for this study have CH_4 as a common species, because we

TABLE 1: Summary of Hydrate Systems Studied

system	hydrate structure	small cavity	large cavity	vapor composition
CH_4	sI	5^{12}	$5^{12}6^2$	$y_{CH_4} = 1.0$
CO_2	sI	5^{12}	$5^{12}6^2$	$y_{CO_2} = 1.0$
C_3H_8	sII	5^{12}	$5^{12}6^4$	$y_{C_3H_8} = 1.0$
$CH_4 + CO_2$	sI	5^{12}	$5^{12}6^2$	$y_{CH_4} = 0.6588$
CH_4 + THF-d_8	sII	5^{12}	$5^{12}6^4$	$y_{CH_4} = 1.0$
$CD_4 + C_3H_8$	sII	5^{12}	$5^{12}6^4$	$y_{CD_4} = 0.6982$
$CH_4 + N_2$	sI	5^{12}	$5^{12}6^2$	$y_{CH_4} = 0.8510$
$CH_4 + C_7D_{14}$	sH[a]	5^{12}	$4^35^66^3$	$y_{CH_4} = 1.0$

[a] Spectra for CH_4 in the large cavity ($5^{12}6^8$) of **sH** have not been observed, either via Raman or NMR spectroscopy.

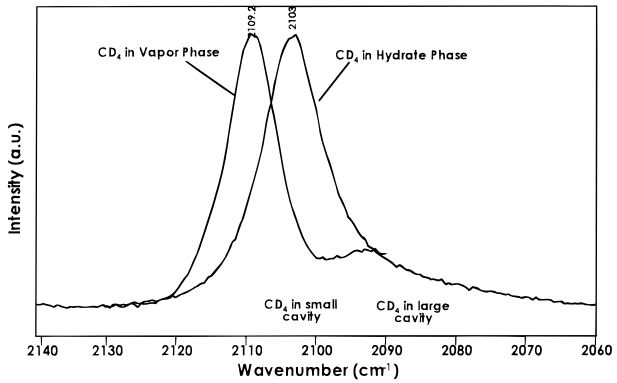

Figure 7. Raman spectra for CD_4 vapor and CD_4 incorporated into the $CD_4 + C_3H_8$ double hydrate. The asymmetric peak shape of CD_4 in the hydrate suggests that a small amount of CD_4 is incorporated in the large cavity of this **sII** $CD_4 + C_3H_8$ hydrate.

wanted to obtain a signature frequency of the CH_4 ν_1 symmetric band in the different cavities of the three hydrate structures (**sI**, **sII** and **sH**). The classification of the hydrates system to their corresponding crystal structure is given in Table 1.

Figure 6 is a compilation of the Raman spectra of the ν_1 symmetric band of CH_4 for all systems studied containing CH_4 as a common hydrate former. It should be pointed out that only the spectra for CH_4, $CH_4 + CO_2$, and $CH_4 + C_7D_{14}$ hydrates were measured at equilibrium conditions. Also shown in Figure 6 is the spectrum for free vapor CH_4 as reference.

All three hydrate crystal structures have the 5^{12} cavity in common and, in addition, one or two larger cavities. CH_4, in principle, can occupy all the cavities in all hydrate structures. The spectrum for CH_4 hydrate (**sI**), as explained earlier, shows occupancy of CH_4 in both cavities of **sI** (5^{12} and $5^{12}6^2$). For the $CH_4 + CO_2$ system, Figure 6 also shows that CH_4 occupies both cavities of **sI**; however, the occupancy of CH_4 in the large cavity ($5^{12}6^2$) is much smaller (the relative intensities of the small to the large bands is decreased as compared to the simple CH_4 hydrate spectrum) since CO_2 only occupies the large cavity. Further evidence for our assignment of the bands was the frequency; CH_4 in the small (5^{12}) cavity occurs at 2915 and at 2905 cm^{-1} in the large ($5^{12}6^2$), for both CH_4 and $CH_4 + CO_2$ hydrate systems.

For the **sII** system, we formed the CH_4 + THF-d_8 double hydrate. THF-d_8 is miscible in water and it can only occupy the large cavity ($5^{12}6^4$) of **sII**. As seen in Figure 6, the corresponding spectrum of CH_4 for this system shows a large band at 2914 cm^{-1}, representing CH_4 in the small **sII** cavity (5^{12}), and a smaller band at 2904 cm^{-1} for CH_4 in the large cavity ($5^{12}6^4$). This assignment of the bands is consistent with that described for the **sI** systems. THF-d_8 occupies most of the large cavities because it has larger Langmuir constant than CH_4. Also, the small cavity of **sII** is the same type as that in

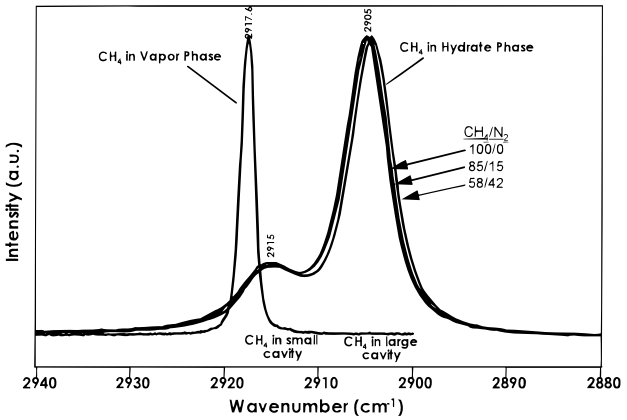

Figure 8. Raman spectra for CH_4 in $CH_4 + N_2$ hydrate. The superposition of the CH_4 bands indicate only **sI** hydrate is found, despite prediction that **sII** is the stable hydrate.

TABLE 2: Frequency of CH_4 Occupancy in the Different Hydrate Crystal Structures

	structure		
condition	I	II	H
small cavity	5^{12}	5^{12}	5^{12}
peak position (cm^{-1})	2915.04 ± 0.58	2913.73 ± 0.76	2912.76 ± 0.30
large cavity	$5^{12}6^2$	$5^{12}6^4$	$4^35^66^3$
peak position (cm^{-1})	2904.85 ± 0.33	2903.72 ± 0.28	2905
no. of spectra measured	164	26	7

sI, and it is positioned at higher frequency relative to the large cavity band (as seen for **sI**).

The Raman spectrum of a **sH** hydrate is shown in Figure 6 for CH_4 in the $CH_4 + C_7D_{14}$ system. **sH** has three cavity types: 5^{12}, $4^35^66^3$, and $5^{12}6^8$. NMR spectroscopy[11] suggest that the help gas (in this case CH_4) only occupies the two small cavities (5^{12} and $4^35^66^3$), because the large cavity ($5^{12}6^8$) is occupied by the large guest molecule and there is only one large cavity per unit cell. The spectrum in Figure 6 clearly shows at least one band for CH_4 in the hydrate, corresponding to CH_4 in the small cavity (5^{12}). The frequency of occurrence of the band for CH_4 in the 5^{12} cavity is again in the vicinity of the 5^{12} bands for **sI** and **sII**.

Table 2 summarizes the information plotted in Figure 6 in terms of the hydrate crystal structure and signature frequency of the ν_1 symmetric band of CH_4 occupancy in the different cavities. A significant number of experiments were performed on **sI** (164), on **sII** (26), and on **sH** (7) to enable a statistical analysis. The statistics in Table 2 suggest the application of Raman spectroscopy as identification tool of the hydrate crystal structure. We should note that the error limits for **sI** and **sII** overlap 0.03 cm^{-1}; however, such overlap is insignificant to precision of the measurements.

We note that the frequency for CH_4 in the 5^{12} cavities of **sI**, **sII**, and **sH** differs by only 1 cm^{-1}, a statistically distinguishable wavenumber, and that this difference is both reproducible and readily measured in Raman studies. By choosing a more rigorous calibration of the monochromator, the accuracy of the frequencies can be measured to 0.01 cm^{-1}. One implication of the difference in frequency of the ν_1 symmetric band of CH_4 in the 5^{12} cavities is that the 5^{12} cavities differ slightly in size from structure to structure, as has been observed by diffraction[2] for **sI** and **sII** clathrates. The frequency shifts are approximately inversely proportional to cavity size for both the 5^{12} and larger cavities.

We also studied two double-hydrate systems at the three-phase equilibrium: $CD_4 + C_3H_8$ (**sII**) shown in Figure 7 and $CH_4 + N_2$ (**sI**) in Figure 8. Both of these systems are of interest

since they are mixtures of components found in natural gas. For the $CD_4 + C_3H_8$ system, CD_4 was used in place of CH_4 because the ν_1 symmetric band of CH_4 and C_3H_8 overlap, and by using CD_4, we were able to separate the CD_4 and C_3H_8 contributions in the hydrate phase. Figure 7 only shows the CD stretch region for CD_4 as free vapor and incorporated in the hydrate lattice. The spectrum for C_3H_8 is not shown but it is identical in features to that in Figure 5.

The Raman spectrum for CD_4 in the hydrate in Figure 7 shows a very broad band with a small shoulder and a long tail at the low wavenumber side. The major band centered at 2103 cm^{-1} corresponds to CD_4 in the small cavity of **sII**, and the shoulder contributing to the long tail is for CD_4 in the large cavity of **sII**. Since C_3H_8 only occupies the large cavity, one expects to find a very small amount of CD_4 in the large cavity, which is consistent with our observations. We also should note that the way we have rationalized the bands for CD_4 in the small and large cavities of **sII** provides additional confirmation of the assignment of the bands for CH_4 in Figure 6. That is, the small cavity (5^{12}) is always at higher wavenumber relative to the large cavity band.

Figure 8 shows the Raman spectrum for CH_4 in the $CH_4 + N_2$ system. This system is important because of possible structural transitions between **sI** and **sII**. X-ray data have shown that N_2 forms type **sII** hydrates,[12] and as shown earlier, CH_4 forms type **sI** hydrates. According to predictions from the statistical thermodynamics model developed by van der Waals and Platteeuw,[13] either **sI** or **sII** hydrates can be formed with $CH_4 + N_2$ as a function of composition of the vapor phase, temperature, and pressure of the system.

We prepared two gas mixtures of $CH_4 + N_2$ that should form **sII**, with $y_{CH_4} = 0.8510$ (borderline composition between **sI** and **sII**) and $y_{CH_4} = 0.5794$ (well inside **sII** region), according to predictions at the conditions of the experiments. Three spectra are shown in Figure 8, and they all superimpose. The three spectra are CH_4 hydrate, $CH_4 + N_2$ hydrate with $y_{CH_4} = 0.8510$, and $CH_4 + N_2$ hydrate with $y_{CH_4} = 0.5794$. All the spectra shown are for measurements at the three-phase equilibrium conditions. Since we do not observe any difference in the relative intensity of the bands and frequency shift of any band, they all suggest the presence of only **sI** hydrate, even though predictions indicate that the equilibrium hydrate structure should be **sII** for both vapor compositions. Unfortunately, an independent experiment, such as X-ray diffraction, was unavailable at the time in order to confirm these results. Recently Kuhs et al.[14] suggested that days to weeks were required for nitrogen hydrates to change from initial **sI** formation to equilibrate to structure II, so our results may have been kinetically limited.

CH_4 Hydrate Composition. Several measurements for CH_4 hydrate were performed at different equilibrium conditions (temperature and pressure) to obtain its composition (i.e., cage occupancy and hydration number). All the spectra collected were identical to Figure 3 for CH_4 hydrate. Because CH_4 partitions between the small and large cavities of **sI**, we were able to deconvolute the band shown in Figure 3 into two mixed Gaussian−Lorentzian bands. The area of the bands represents the amount of CH_4 in each cavity. The deconvolution of the bands were accomplished with the curve-fitting routine in the commercial package GRAMS/386 from Galactic Industries Corporation. This procedure allowed us to determine the ratio of areas of the small to the large band, and after accounting for the fact that there are three times as many large as small cavities in **sI**, we obtained the occupancy ratio $\theta_{s,CH_4}/\theta_{l,CH_4}$.

In order to determine the absolute occupancy of CH_4 in the small and large cavities, we were required to invoke the statistical thermodynamics expression for the chemical potential $\mu_w(h)$ of water molecules in a **sI** hydrate,

$$\mu_w(h) - \mu_w(h^\circ) = \frac{RT}{23}[3\ln(1-\theta_{l,CH_4}) + \ln(1-\theta_{s.CH_4})] \quad (4)$$

where $\mu_w(h^\circ)$ is the chemical potential of a hypothetical empty lattice, and θ_s and θ_l the fractional occupancy of large and small cavities, respectively. Equation 4 assumes (i) the free energy of the hydrate is independent of cavity occupation, (ii) each cavity can be occupied by only one guest molecule and the guest molecules cannot diffuse from the cavity, (iii) there are no guest−guest interactions and host−lattice distortions, (iv) classical statistics are valid, and (v) no quantum effects need to be considered. If we assume the hydrate is in equilibrium with ice, we can rewrite eq 4 by subtracting the chemical potential of ice from either side to obtain an expression in terms of changes in the chemical potential, as

$$\Delta\mu_w(h) - \Delta\mu_w(h^\circ) = \frac{RT}{23}[3\ln(1-\theta_{l,CH_4}) + \ln(1-\theta_{s,CH_4})] \quad (5)$$

$\Delta\mu_w(h)$ can be derived and calculated from classical thermodynamics and $\Delta\mu_w(h^\circ)$ for **sI** has been reported and confirmed by several research groups.[15,16] The value for $\Delta\mu_w(h^\circ)$ used in the calculation was 1297 J/mol.

Therefore, by combining eq 5 and the measured occupancy ratio $\theta_{s,CH_4}/\theta_{l,CH_4}$, the occupancy of the small and large cavities by CH_4 were determined. The results are shown in Table 3, as well as the values predicted by the statistical thermodynamics model. The column labeled *n* in Table 3 corresponds to the hydration number calculated from the occupancies by the following expression:

$$n = \frac{23}{3\theta_{l,CH_4} + \theta_{s,CH_4}} \quad (6)$$

The value for the hydration number is in agreement with other values reported in the literature that range from about 5.8 to 6.3.[17−21] The results in Table 3 also show that the large cavities are almost filled, whereas the small cavities are about 90% filled.

TABLE 3: Cage Occupancy and Hydration Number for CH_4 Hydrate

	experimental			statistical thermodynamic model		
T (K)[a]	θ_L	θ_S	n	θ_L	θ_S	n
273.65	0.971	0.920	6.00	0.974	0.876	6.06
σ (5)[b]	±0.002	±0.021	±0.02			
274.65	0.972	0.899	6.03	0.975	0.882	6.04
σ (5)[b]	±0.002	±0.020	±0.02			
275.65	0.974	0.869	6.07	0.976	0.887	6.03
σ (6)[b]	±0.002	±0.028	±0.04			
276.65	0.973	0.866	6.07	0.978	0.892	6.01
σ (3)[b]	±0.000	±0.005	±0.01			

[a] Measurement performed at equivalent equilibrium pressure at given temperature. [b] Number of measurements.

$CH_4 + CO_2$ Hydrate Composition. Figure 9 shows the Raman spectra for CH_4 and the $CH_4 + CO_2$. Spectra were collected at several sets of equilibrium pressure and temperature conditions for two vapor compositions as listed in Table 4. In order to obtain the hydrate guest composition, integration of the areas under the curves for the CH_4 band and CO_2 band were calculated using the single-peak integration routine in GRAMS/386. The limits of integration for CH_4 were from 2940 to 2880 cm^{-1} and, for CO_2, from 1420 to 1340 cm^{-1} and 1305 to 1245 cm^{-1}. Once the areas were known, concentrations of CH_4 and

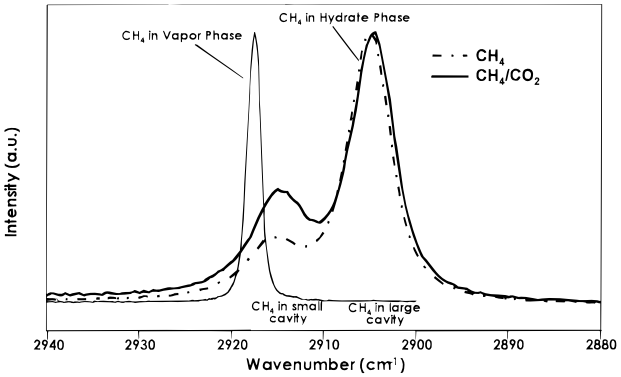

Figure 9. Raman spectra for CH_4 vapor and CH_4 incorporated into $CH_4 + CO_2$ hydrate. The relative differences in band intensities for the large and small cavities was used to calculate hydrate composition.

TABLE 4: Hydrate Guest Composition for $CH_4 + CO_2$ System

	T (K)				
	273.15	274.15	275.15	277.15	278.15
		$y_{CH_4} = 0.4255$			
x_{CH_4} experimental	0.254	0.270		0.286	0.294
σ	± 0.024 (5)[a]	±0.009 (4)		±0.013 (4)	±0.013 (3)
x_{CH_4} predicted	0.268	0.271		0.281	0.285
		$y_{CH_4} = 0.6588$			
x_{CH_4} experimental	0.451	0.451	0.466		0.477
σ	±0.015 (6)	±0.006 (3)	±0.004 (3)		±0.011 (4)
x_{CH_4} predicted	0.473	0.477	0.480		0.492

[a] Value in parentheses represents number of measurements.

CO_2 in the hydrate were determined by applying the calibration curve (Figure 2). Table 4 shows the hydrate guest compositions (and standard deviations) for two vapor compositions measured at several temperatures, with pressures within 5% of predicted equilibrium pressure. Also shown in Table 4 are the compositions predicted by the statistical thermodynamics model.

Good agreement with the measured hydrate guest composition is evidence that the model developed by van der Waals and Platteeuw gives acceptable predictions of the hydrate phase. The results also suggest that the assumption made about the Raman scattering cross section is valid to the extent of measurement uncertainty.

The spectra also enabled the determination of the occupancy of CH_4 in the small and large cavities of **sI** hydrate; CO_2 was found to occupy only the large cavity of **sI**. It is clear from Figure 9 that CH_4 partitions between the small and large cavities. By using the curve fitting routine in GRAMS/386, we deconvoluted the CH_4 band into two mixed Gaussian−Lorentzian bands. This approach allowed us to separate the areas contributing to CH_4 in the small and large cavities and to subsequently calculate the relative ratios of occupancy $\theta_{s,CH_4}/\theta_{l,CO_2}$ and $\theta_{l,CH_4}/\theta_{l,CO_2}$ by application of the calibration curve (Figure 2).

In order to obtain the occupancy of CO_2 in the large cavity and CH_4 in both cavities, we turned to the statistical thermodynamics expression from van der Waals and Platteeuw model, the same way as done to obtain the occupancies in CH_4 hydrate:

$$\mu_w(h) - \mu_w(h^\circ) = \frac{RT}{23}[3\ln(1 - \theta_{l,CO_2} - \theta_{l,CH_4}) + \ln(1 - \theta_{s,CH_4})] \quad (7)$$

By assuming ice as the reference state, eq 7 can be subtracted from an equality of the chemical potential of water in the ice phase and rewritten as

$$\Delta\mu_w(h) - \Delta\mu_w(h^\circ) = \frac{RT}{23}[3\ln(1 - \theta_{l,CO_2} - \theta_{l,CH_4}) + \ln(1 - \theta_{s,CH_4})] \quad (8)$$

$CH_4 + CO_2$ also forms **sI** hydrate; therefore, the same value (1297 J/mol) for $\Delta\mu_w(h^\circ)$ was used as before.

This procedure allowed us to calculate the occupancies as presented in Tables 5 and 6. Also presented in Tables 5 and 6 are the hydration numbers calculated from

$$n = \frac{23}{3\theta_{l,CO_2} + 3\theta_{l,CH_4} + \theta_{s,CH_4}} \quad (9)$$

The results in Tables 5 and 6 show that almost all the large cavities are filled, whereas only a small fractional of the small cavities are filled by CH_4. One should also note an increasing occupancy of CH_4 in both large and small cavities as the temperature increases (pressure is also increasing since measurements were at equilibrium). The implication of this observation is that, at higher pressures, more of the volatile component is incorporated in the hydrate (see also compositions presented in Table 4), thus causing a smaller hydration number. Note that the hydrate guest compositions determined in Table 4 are independent of the statistical thermodynamics model, whereas the occupancies in Tables 5 and 6 assume the validity of the model.

TABLE 5: Cage Occupancy and Hydration Number for $CH_4 + CO_2$ System; $y_{CH_4} = 0.4255$

T (K)	θ_{l,CO_2}	θ_{l,CH_4}	θ_{s,CH_4}	n
273.15	0.812	0.175	0.126	7.45
σ	±0.024	±0.023	±0.008	±0.02
274.15	0.804	0.183	0.137	7.43
σ	±0.007	±0.007	±0.006	±0.01
277.15	0.790	0.195	0.144	7.42
σ	±0.011	±0.011	±0.006	±0.01
278.15	0.787	0.197	0.147	7.42
σ	±0.008	±0.008	±0.008	±0.02

TABLE 6: Cage Occupancy and Hydration Number for $CH_4 + CO_2$ System; $y_{CH_4} = 0.6588$

	T (K)			
	θ_{l,CO_2}	θ_{l,CH_4}	θ_{s,CH_4}	n
273.15	0.632	0.355	0.190	7.30
σ	±0.017	±0.017	±0.009	±0.02
274.15	0.629	0.358	0.184	7.32
σ	±0.006	±0.006	±0.005	±0.01
275.15	0.614	0.372	0.198	7.29
σ	±0.004	±0.004	±0.002	±0.00
278.15	0.604	0.381	0.208	7.27
σ	±0.007	±0.007	±0.005	±0.01

Conclusions

This work demonstrates that Raman spectroscopy is a valuable analytical tool for investigating the properties of the clathrate hydrate phase at in-situ temperature and pressure conditions. In addition, we have shown that Raman spectroscopy can give similar information to that obtained from NMR spectroscopy, often considered as a standard technique in hydrate studies. However, Raman spectroscopy is simpler and less resource intensive, compared to the NMR technique.

The vibrational spectra of several single and double hydrate guests were shown to be changed when they are incorporated into the hydrate lattice, both in terms of position and band shape. The frequency of the CH_4 band in the hydrate provides a

signature for a specific crystal structure, suggesting that the Raman technique can be used to identify the hydrate crystal structure.

Cage occupancies and hydration numbers for CH_4 hydrate at several equilibrium conditions were calculated from the ratio of the areas corresponding to the small and large cavities.

The large cages are almost fully occupied and the small cages were about 90% occupied by CH_4.

Hydrate compositions were measured for two vapor compositions of $CH_4 + CO_2$ mixture at several equilibrium conditions at or above the ice point. The experimental values obtained for the hydrate composition are in good agreement with those values predicted by the statistical thermodynamics model, thus providing a validation of the model. Hydration numbers were indirectly determined from the occupancy of CH_4 in the small and large cavities of **sI**; CO_2 was only measured as an occupant in the large cavity. These results were the first direct measurement of the hydrate guest composition

One important result is the ability to obtain key thermodynamic parameters, such as $\Delta\mu^\circ$, which are otherwise hard to measure by other current means. The Raman technique can enable determination of the relative occupancy of cavities for a particular structure. This information, combined with measurement of hydration number *n*, can then be used to obtain the absolute occupancies of the cavities, which in turn are used to calculate $\Delta\mu^\circ$.

The fact that Raman spectroscopic studies are possible at in-situ temperature and pressure conditions, combined inherent simplicity of optical spectroscopy, suggests that this technique can be used for industrial process monitoring of hydrate formation.

Acknowledgment. The National Science Foundation provided funding for this work through a Small Exploratory Research Grant CTS-9527420. We are very grateful to Professor T. E. Furtak for advice regarding consistency of the Raman scattering cross section. The assistance of Shiva Subramanian with the statistical analysis of peak positions is greatly appreciated. This work was initiated under a CRADA agreement between the U.S. Geological Survey and the Center for Hydrate Research, Colorado School of Mines.

References and Notes

(1) Long, X. Master Thesis, Colorado School of Mines, 1994.
(2) Sloan, E. D. *Clathrate Hydrates of Natural Gases*; Marcel Dekker, Inc.: New York, 1990.
(3) Long, D. A. *Raman Spectroscopy*; McGraw-Hill: New York, 1977.
(4) Wopenka, B.; Pasteris, J. D. *Appl. Spectrosc.* **1986**, *40*, 144.
(5) Wopenka, B.; Pasteris, J. D. *Anal. Chem.* **1987**, *59*, 2165.
(6) Placzek, G. *Handbuch der Radiologie*; Marx, E., Ed.; Akademische Verlagsgesellschaft: Leipzig, 1934; Vol. 2, p 209.
(7) Schrötter, H. W.; Klöckner, H. W. In *Raman Scattering Cross Sections in Gases and Liquids*; Weber, A., Ed.; Springer-Verlag: New York, 1979; p 123.
(8) Seitz, J. C.; Pasteris, J. D.; Wopenka, B. *Geochim. Cosmochim. Acta* **1987**, *51*, 1651.
(9) Ratcliffe, C. I.; Ripmeester, J. A. *J. Phys. Chem.* **1986**, *90*, 1259.
(10) Fleyfel, F.; Devlin, J. P. *J. Phys. Chem.* **1988**, *92*, 631.
(11) Ripmeester, J. A.; Ratcliffe, C. I.; Tse, J. S. *J. Chem. Soc., Faraday Trans. 1* **1988**, *84*, 3731.
(12) Davidson, D. W.; Handa, Y. P.; Ratcliffe, C. I.; Tse, J. S.; Powell, B. M. *Nature* **1984**, *311*, 142.
(13) van der Waals, J. H.; Platteeuw, J. C. *Adv. Chem. Phys.* **1959**, *2*, 1.
(14) Kuhs, W., Chazallon, B., Radaelli, P., Pauer, F., Kipfstuhl, J., *Proceedings of the 2nd International Conference on Natural Gas Hydrate*, Toulouse, France, June 2−6, 1996; p 9.
(15) Davidson, D. W.; Handa, Y. P.; Ripmeester, J. A. *J. Phys. Chem.* **1986**, *90*, 6549.
(16) Dharmawardhana, P. B.; Parrish, W. R.; Sloan, E. D. *Ind. Eng. Chem. Fundam.* **1980**, *19*, 410.
(17) Ripmeester, J. A.; Ratcliffe, C. I. *J. Phys. Chem.* **1988**, *92*, 337.
(18) Glew, D. N. *J. Phys. Chem.* **1962**, *66*, 605.
(19) Gallaway, T. J.; Ruska, W.; Chappelear, P. S.; Kobayashi, R. *Ind. Eng. Chem. Fundam.* **1970**, *9*, 237.
(20) Handa, Y. P. *J. Chem Thermodyn.* **1986**, *18*, 915.
(21) De Roo, J. L.; Peters, C. J.; Lichtenthaler, R. N.; Diepen, G. A. M. *AIChE J.* **1983**, *29*, 651.